# Effects of Backbone and Side Chain on the Molecular Environments of Chiral Cavities in Polysaccharide-Based Biopolymers

Rahul B. Kasat, Nien-Hwa Linda Wang, and Elias I. Franses*

*School of Chemical Engineering, Purdue University, 480 Stadium Mall Drive, West Lafayette, Indiana 47907-2100.*

*Received January 2, 2007; Revised Manuscript Received March 6, 2007*

The effects of the backbone and side chain on the molecular environments in the chiral cavities of three commercially important polysaccharide-based chiral sorbents—cellulose tris(3,5-dimethylphenylcarbamate) (CDMPC), amylose tris(3,5-dimethylphenylcarbamate) (ADMPC), and amylose tris[(*S*)-α-methylbenzylcarbamate] (ASMBC)—are studied by attenuated total reflection infrared spectroscopy (ATR-IR), X-ray diffraction (XRD), $^{13}$C cross-polarization/magic-angle spinning (CP/MAS) and MAS solid-state NMR, and density functional theory (DFT) modeling. These sorbents are used widely in preparative-scale chiral separations. ATR-IR is used to determine how the H-bonding states of the C═O and NH groups of the polymer depend on the backbone and side chain. The changes in the polymer crystallinity are characterized with XRD. The changes in the polymer helicity and molecular mobility for polymer-coated silica beads (commercially called Chiralcel OD, Chirapak AD, and Chiralpak AS) are probed with $^{13}$C CP/MAS and MAS solid-state NMR. The IR wavenumbers and the NMR chemical shifts for the polymer backbone monomers and dimers and the side chains are predicted at the DFT/B3LYP/6-311+g(d,p) level of theory. It is concluded that the molecular environments of the C═O, NH, and phenyl groups show significant differences in intramolecular and intermolecular interactions and in the nanostructures of the chiral cavities of these biopolymers. These results have implications for understanding how the molecular environments of chiral cavities of these polymers affect their molecular recognition mechanisms.

## 1. Introduction

The mechanism of the molecular recognition of solutes by substrates or sorbents plays a crucial role in many chemical and biological systems.[1] An important area is enantiorecognition or chiral discrimination.[2] The importance of pharmaceutical chiral separations has grown significantly in the past decade after the FDA decided to require that racemic drug mixtures must be separated and that individual enantiomers must be tested separately for their pharmacokinetic and pharmacodynamic effects.[3] Many types of chiral stationary phases (CSPs)—proteins, antibiotics, cyclodextrins, polysaccharides, Pirkle phases, etc.—have significant selectivities, or selective "molecular recognition", of enantiomers of chiral solutes.[4−8] Certain polysaccharide-based biopolymers, first developed by Okamoto and co-workers,[9,10] have been quite successful in separating a wide variety of chiral molecules.

Among such sorbents, the following three chiral sorbents have been chosen for study: cellulose tris(3,5-dimethylphenylcarbamate) (CDMPC), amylose tris(3,5-dimethylphenylcarbamate) (ADMPC), and amylose tris[(*S*)-α-methylbenzylcarbamate] (ASMBC) (Figure 1). These sorbents are widely used in analytical and preparative chiral separations due to their versatility and effectiveness.[10−12] These polymers are normally used as thin films deposited on porous silica beads. ADMPC and CDMPC have the same side chains but different backbones (Figure 1). The former, being amylose-based, has α-D-(1→4) linkages, while the latter, being cellulose-based, has *β*-D-(1→4) linkages. ADMPC and ASMBC have the same α-D-(1→4) amylose backbone linkages but different side chains. The side chain of ADMPC has no chiral center, and that of ASMBC has one chiral center (Figure 1). The rather large side chains seem to generate nanometer-sized molecular cavities in the polymer structures (Figure 2). The predicted cavities in these polymers show significant differences in their sizes and steric environments. In addition to steric hindrances, these cavities allow H-bonding and dipole−dipole interactions of polymer carbamate groups with solute or solvent functional groups, and phenyl−phenyl interactions of the phenyl rings with the solute phenyl groups.[9] The molecular environments of such "chiral" cavities may be different for different polymers and appear to be related to the chiral recognition mechanisms, which for these polymers have not been completely elucidated.[9]

Toward that objective, and since the detailed crystal structures of these polymers have not been solved, a fundamental study of the molecular environments of the "chiral" cavities in these biopolymers in detail is desired. Multiple direct experimental techniques, including infrared spectroscopy (IR), X-ray diffraction (XRD), and solid-state NMR, and also density functional theory (DFT) modeling are used. Attenuated total reflection infrared spectroscopy (ATR-IR) on polymer films is used primarily for elucidating the H-bonding states of the C═O and NH groups in these polymers. The IR wavenumbers are compared with the wavenumbers of the optimized side chain structures calculated from DFT. The variations in the polymer crystallinity are studied by XRD. And finally, $^{13}$C CP/MAS and MAS (magic-angle spinning, with and without cross-polarization) solid-state NMR spectra for CDMPC-polymer-coated silica beads (Chiralcel OD), ADMPC-polymer-coated silica beads (Chiralpak AD), and ASMBC-polymer-coated silica beads (Chiralpak AS) are obtained to further elucidate the differences

* Author to whom correspondence should be addressed. Phone: +1-765-494-4078. Fax: +1-765-494-0805 E-mail: franses@ecn.purdue.edu.

10.1021/bm070006h CCC: $37.00 
Published on Web 04/18/2007

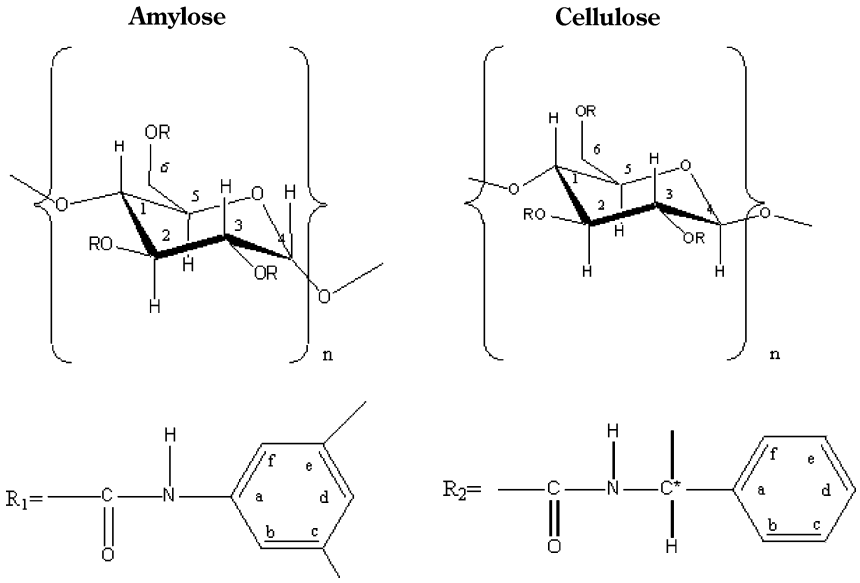


**Figure 1.** Amylose tris(3,5-dimethylphenylcarbamate) (ADMPC) (R = $R_1$), amylose tris[(*S*)-α-methylbenzylcarbamate] (ASMBC) (R = $R_2$), and cellulose tris(3,5-dimethylphenylcarbamate) (CDMPC) (R = $R_1$). Amylose has α-D-(1→4) linkages and cellulose has β-D-(1→4) linkages. An asterisk indicates the chiral center.

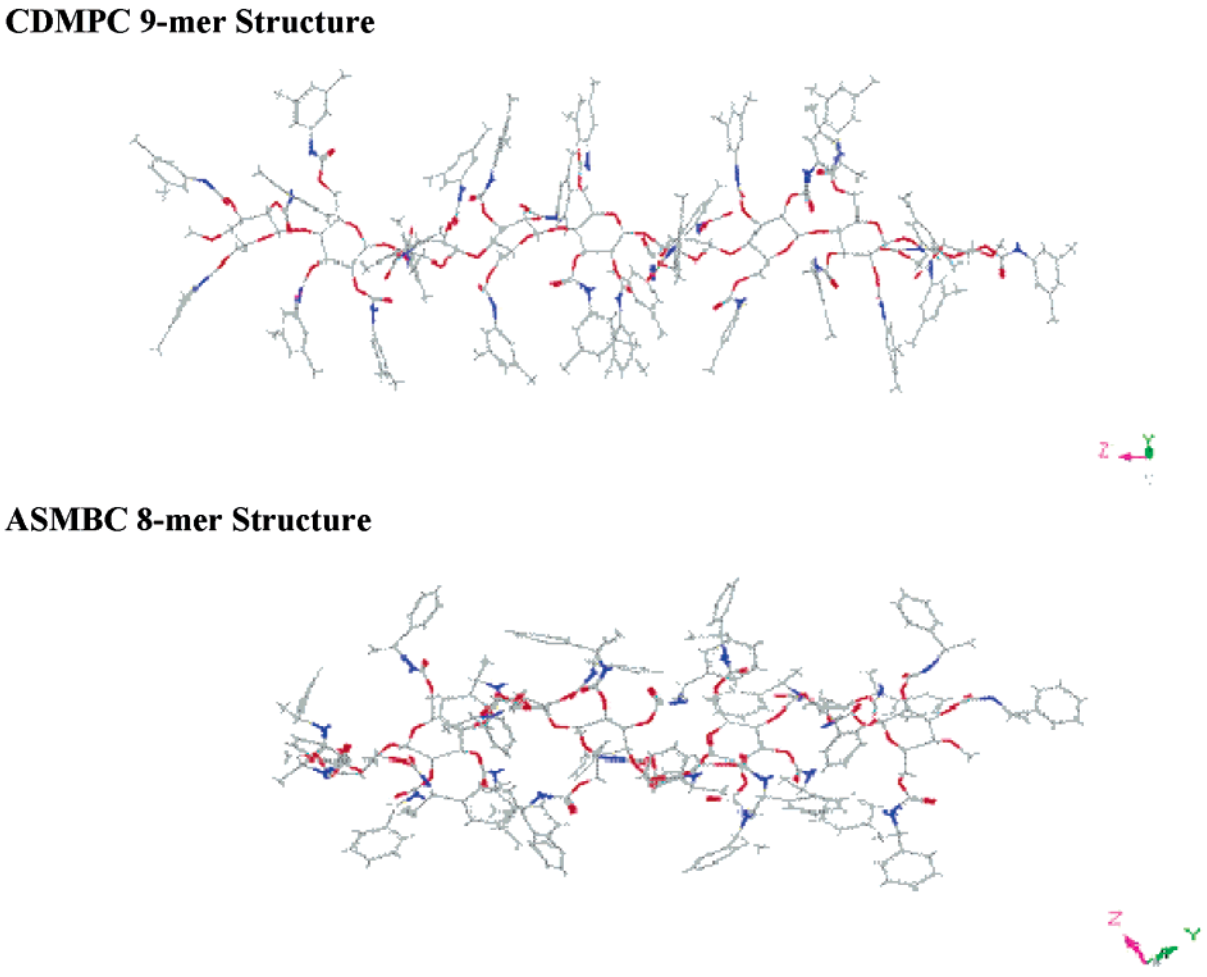


**Figure 2.** Three-dimensional structures of a CDMPC 9-mer rod and an ASMBC 8-mer rod generated by Materials Studio (see section 2.5). The predicted rods contain several nanometer-sized cavities between the side chains.

in the polymer backbone and side chain structures and their molecular mobilities. The NMR chemical shifts are compared with DFT simulated chemical shifts of the optimized backbone and side chain structures. These results are important for better understanding of the C═O, NH, and phenyl functional groups, resulting in better insights into the molecular environments of the chiral cavities.

Many literature studies report the successful use of these polymers in the chromatographic separations of numerous chiral solutes.[13−19] The effect of additives on the chiral separations

of various solutes by use of these polymers was extensively studied.[11,20] Reversals in elution orders of some of the racemic compounds were sometimes observed by changing the polymer sorbent.[21,22] Wainer and co-workers[23] developed structure−retention correlations by measuring the retention times and selectivities of a series of amides on three amylose-based CSPs. They concluded that the elution order of the solutes depended on the amylose backbone chirality, while the selectivity was affected by the side chain chirality. The differences in the enantioseparation of racemates by the phenylcarbamates of amylose and cellulose were ascribed to "differences in their higher-order structures".[9] For the cellulose tris(phenylcarbamates), Vogt and Zugenmaier[24] have proposed a 3-fold (3/2) helical conformation. Okamoto and co-workers[25] also proposed a similar helical conformation for CDMPC using molecular mechanics calculations. For the amylose tris(phenylcarbamates), Vogt and Zugenmaier[26] have proposed a 4-fold helical conformation. On the basis of their solid-state NMR results, Wenslow and Wang[27] proposed that the ADMPC has a helical structure less than 6-fold.[27] From 2D solution-state NMR and molecular modeling of the ADMPC polymer with a lower degree of polymerization, Okamoto and co-workers[28] proposed a left-handed 4-fold (4/3) structure,[28] in which the glucose residues lie along the helical axis while the side chains form chiral grooves in which the chiral solutes enter and interact. The variations in the helical conformations are related to the changes in the molecular environments of the sorbent chiral cavities. Chankvetadze et al.[29,30] studied various phenylcarbamate derivatives of amylose and cellulose by IR, $^1$H solution-state NMR, and circular dichroism (CD). They concluded that the chromatographic elution order and selectivity of chiral solutes depend on the positions of different substituents on the phenyl groups. They correlated the chiral recognition ability of the stationary phase with the NMR chemical shifts of NH protons and the IR wavenumber shifts of the NH band.

Wenslow and Wang[27,31] attributed the elution order reversal and other unusual retention behavior to differences in the molecular environments of the chiral cavities in the polymer structure due to the alcohol modifiers. Our group recently studied the effects of the solvent (or "mobile phase") on the structure of the ADMPC polymer by IR, NMR, XRD, and DFT modeling.[32] It was found that the H-bonding states of the ADMPC polymer change upon absorption of polar solvents and usually result in an increase of both the polymer crystallinity and the side chain mobility.[32] By use of IR and DFT modeling, the chromatographic retention times of simple nonchiral solutes with ADMPC polymer were also interpreted.[33] Here, for the first time the structure of the ADMPC is compared to that of two related polymers, CDMPC (different backbone, same side chain) and ASMBC (different side chain, same backbone) by direct experimental techniques and DFT modeling, to establish the backbone and side chain effects on the nanostructures of the dry polymers. The main objective of this study is to elucidate the molecular environments of the chiral cavities (Figure 2), which play important roles in the chiral discrimination mechanism of these polymers. Future studies may focus on the structure modification by solvents and various chiral solutes interacting with these polymers.

## 2. Materials and Methods

**2.1. Materials.** CDMPC-polymer-coated silica beads (Chiralcel OD), ADMPC-polymer-coated silica beads (Chiralpak AD), and ASMBC-polymer-coated silica beads (Chiralpak AS) were provided by Chiral Technologies, Inc. (Exton, PA). *N*,*N*-dimethylformamide (DMF), *N*,*N*-dimethylacetamide (DMAc), and tetrahydrofuran (THF) were purchased from Mallinckrodt Chemicals (Phillipsburg, NJ). Tetramethylsilane (TMS) and glycine were purchased from Sigma−Aldrich (Milwaukee, WI).

**2.2. ATR-FTIR Spectroscopy.** Polymer films for ATR-IR experiments were prepared as follows. Each polymer was dissolved in THF at 60 °C, and the solution was cooled to room temperature. The polymer was spin-coated on Si-ATR plates (Wilmad, NJ) by use of a WS-400A-6NPP-Lite spin processor (Laurell Technologies Corp.), at a spinning speed of 500 rpm for 5 min. The film thicknesses were about 1−10 $\mu$m. The films were annealed in a vacuum oven for at least 1 h at 80 °C. A Nicolet Protégé 460 Fourier transform infrared spectrometer (Thermo Scientific), equipped with a mercury−cadmium−telluride (MCT) detector cooled with liquid nitrogen, was used to obtain all Fourier transform infrared (FTIR) spectra. Spectral contributions from water vapor and carbon dioxide were minimized by continuously purging from a Balston purge gas generator (Parker, MA). ATR spectra were collected with unpolarized incident light at 25 °C by use of a custom-made ATR accessory. Each experiment was reproduced at least twice. All spectra were taken at a resolution of 2 $cm^{-1}$ with Happ−Genzel apodization. Even though the Si-ATR plate has an absorption cutoff at about 1500 $cm^{-1}$, spectra down to ca. 1000 $cm^{-1}$ were still collected reliably because of the large sample thickness, and were the same as those obtained with a plate made of Ge, which has a cutoff of ca. 800 $cm^{-1}$. All spectra were collected from 256 scans. The IR spectra of the polymer films prepared with DMAc and DMF as solvents are identical to that obtained with THF and are not shown here. These spectra are also independent of the annealing conditions used in preparing the polymer films.

**2.3. Wide-Angle X-ray Diffraction.** Dry polymer films were cast from THF on glass slides at 80 °C in an oven. A wide-angle (angles ranging from 3° to 50°) X-ray instrument (Bruker, Madison, WI) was used at room temperature with Cu K$\alpha$ beam radiation of 0.154 nm. The scan rate was 1 deg/min with a step size of 0.05. Identical patterns are observed for the films produced from DMF or DMAc solvent. These spectra are also independent of the annealing conditions used.

**2.4. Solid-State NMR.** $^{13}$C CP/MAS and MAS spectra were obtained for the three polymers coated on silica beads; Chiralcel OD, Chiralpak AD, and Chiralpak AS. The experiments were performed on a 400 MHz NMR spectrometer CMX-Infinity (Varian, CA), equipped with a Chemagnetics DR-T3 MAS probe operating at 100.61 MHz for $^{13}$C. Experiments were done with a 0.8 ms contact time and a 5 s pulse delay. The pulse sequences used in the experiments were from the Spinsight software package (Varian, CA). The spinning frequency was 8 kHz. All $^{13}$C spectra were referenced to TMS (0 ppm) and to glycine (176.03 ppm) as a secondary reference.

**2.5. Computational Details.** An estimate of the polymer structure was obtained as follows. A 8-mer ASMBC polymer rod with 4-fold helix and a 9-mer CDMPC polymer rod with 3-fold helix were constructed by use of linked-atom least-squares (LALS).[25,28,34] These structures were then energy-minimized via the molecular mechanics (MM) simulations, which were done by using the Discover module from the Materials Studio Modeling 3.0 software (Accelrys, CA).[35] The force field used in these calculations was PCFF (polymer-consistent force field).[36] Different starting guesses can yield different local minima instead of a global minimum. In this study, different initial guesses yielded similar structures qualitatively. No quantitative predictions from the MM calculations are reported here.

The Gaussian 03 program was used for ab initio electronic structure calculations of the single side chains.[37] Only one side chain was simulated, to avoid time-consuming calculations of monomers or oligomers containing large numbers of atoms, in order to obtain certain predictions of the structures. The results were used to calculate the IR wavenumbers of the amide I−III bands, phenyl bands, and other groups of the polymer side chains and the $^{13}$C chemical shifts for the optimized structures.

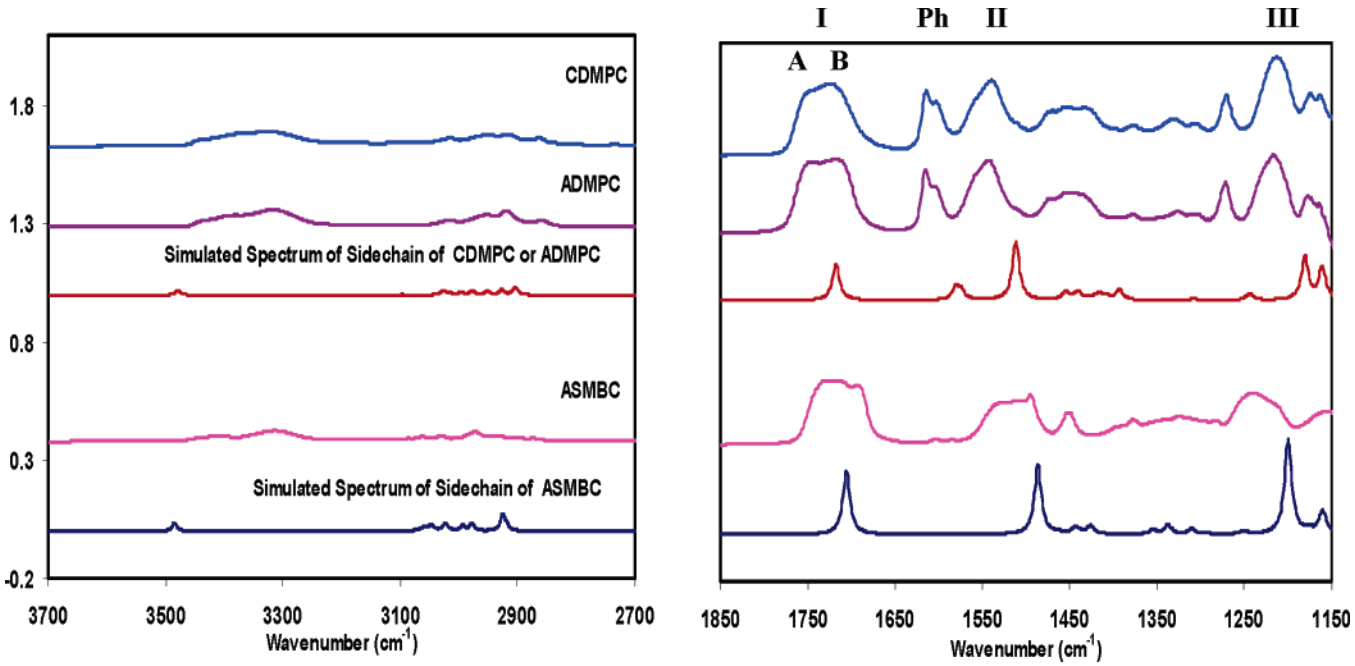


**Figure 3.** Experimental IR spectra of all the polymers and simulated IR spectra of polymer side chains at the DFT/B3LYP/6−311+g(d,p) level of theory. Spectra are shifted vertically to avoid overlap; there are no significant lines due to the side chains between 2700 and 1850 $cm^{-1}$.

**Table 1.** Measured and Predicted IR Wavenumbers for Different Amide and Phenyl Bands of Dry Polymers[a]

| | IR wavenumbers ($cm^{-1}$) | | | |
|---|---|---|---|---|
| system | amide I | phenyl peaks | amide II | amide III |
| CDMPC | 1744 (A), 1725 (B) | 1614, 1603 | 1540 | 1213 |
| ADMPC | 1745 (A), 1717 (B) | 1615, 1604 | 1542 | 1215 |
| *predicted for ADMPC/CDMPC side chain* | *1717 (312)* | *1581 (103), 1575 (72)* | *1512 (500)* | *1181 (364)* |
| ASMBC | 1731[b] (br) (A), 1696[b] (B) | 1604, 1583 | 1507−1527 (br) | 1240 (br) |
| *predicted for ASMBC side chain*[c] | *1702 (329), 1710 (409)* | *1578 (5), 1559*[d] *(1)* | *1471 (385), 1476 (445)* | *1186 (302), 1189 (331)* |

[a] IR wavenumbers and intensities for amide I−III and phenyl bands of polymer side chains are predicted at the DFT/B3LYP/6-311+g(d,p) level of theory (shown in italic type). Predicted IR intensities are given in parentheses. Predicted IR wavenumbers are corrected by a scaling factor of 0.96. br, broad. [b] A third peak at 1717 $cm^{-1}$ is also observed. [c] DFT predicts two conformers with a small energy difference. [d] The phenyl band wavenumbers of the two ASMBC conformers are nearly the same.

The geometry optimization calculations for minimum energy were performed by nonlocal gradient-corrected density functional theory (DFT). The structures of single side chains for CDMPC or ADMPC and for ASMBC were optimized at the DFT/B3LYP/6-311+g(d,p) level of theory. The B3LYP hybrid functional,[38] which includes a mixture of Hartree−Fock exchange with DFT exchange-correlation functional, gives intermolecular geometries and IR wavenumbers similar to those obtained from MP2.[39] Basis sets at the 6-311+g(d,p) level (triple-ζ level) have polarization functions on non-hydrogen and hydrogen atoms and diffused functions with diffuse sp shell on non-hydrogen atoms.[40] With a scaling factor of 0.96, the calculated IR wavenumbers give significantly better accuracy with triple-ζ basis sets compared to double-ζ basis sets.[41] The ab initio $^{13}C$ chemical shieldings of cellulose, amylose, amylose acetate, and cellulose acetate monomers were computed with the gauge-including atomic orbital (GIAO) method by use of DFT theory and the 6-311+g(d,p) basis set. The results were scaled with the chemical shielding computed at the B3LYP/6-311+g-(2d,p) GIAO level of theory for the methyl carbons of tetramethylsilane (TMS). The dimers of cellulose (3-fold helical conformation), and amylose (4-fold helical conformation) were generated by linked-atom least-squares (LALS)[34] and optimized with Gaussian for prediction of the chemical shifts.

## 3. Results and Discussion

### 3.1. ATR-IR Results and DFT Wavenumber Predictions.

*3.1.1. Effect of Backbone: CDMPC versus ADMPC.* For CDMPC, different coating solvents can result in slightly different chromatographic enantioselectivities, but the effects are not as pronounced as for triacetylcellulose or cellulose tribenzoate.[42] It is found that the IR spectra are independent of the coating solvent used (see section 2.2). Any small conformational change possibly due to the change in coating solvent does not result in any significant difference in the IR spectra. The IR spectra of CDMPC and ADMPC are shown in Figure 3. The ADMPC spectrum was analyzed in detail previously[32,33] and is shown here to enable comparisons. The main focus is in the 1800−1500 $cm^{-1}$ region, because the C═O, NH, and phenyl groups, which are part of the chiral cavities, have IR bands in this region. Also, the effects of solvents or simple solutes on the ADMPC polymer structure can be studied in this region without significant overlap from the solvent or solute peaks.

For CDMPC, the broad peak in the region 1750−1700 $cm^{-1}$ is due to amide I, which results from 80% C═O stretching and 20% NH bending vibrations.[43] This band (Table 1) shows two broad overlapping peaks, which are termed A and B. The peaks are shifted from the (assumed) wavenumber of "free" groups taken at ca. 1790 $cm^{-1}$ at the band edge due to the well-known effect of H-bonding on the C═O stretching vibrations.[43] Band B is assigned mainly to C═O relatively "strongly H-bonded" to NH, and band A is assigned mainly to C═O relatively "weakly H-bonded" to NH (Figure 1), while each band is so broad that it must include a distribution of H-bonding strengths.

The weakly H-bonded C═O can also have contributions from likely dipole−dipole and van der Waals interactions with the neighboring side chains in the same monomer or polymer or from adjacent polymer chains. Similar trends are observed for the amide I band for dry ADMPC polymer, which has the same side chain as CDMPC but an amylose backbone.[32,33] It has been postulated that the strongly H-bonded band B arises mainly from intrapolymer interactions (Figure 2), while the weakly H-bonded band A arises from weaker intrapolymer interactions and also possibly from some interpolymer interactions among interpenetrating chains.[32,33]

Since the wavenumber of band A for amide I is the same in CDMPC as in ADMPC, and the wavenumber of band B is larger (by 8 $cm^{-1}$) in CDMPC (Table 1), it is concluded that the strongly H-bonded H-bonds of C═O are slightly weaker in CDMPC. The small differences reflect the backbone effect on the supramolecular packing at the nanoscale. With a possible 3-fold helix and ca. 15 Å helical pitch, CDMPC has a rise per residue of ca. 5 Å.[25] By contrast, with a possible 4-fold helix and ca. 16 Å helical pitch, ADMPC has a rise per residue of ca. 4 Å.[28] It is postulated that the higher the rise per residue, the weaker the intrapolymer H-bonding interactions between side chains, resulting in weaker H-bond interactions.

The DFT-simulated IR spectrum for one side chain of either CDMPC or ADMPC polymer, corresponding to completely free amide groups with no intra- or interpolymer H-bonds (section 2.4), is also shown in Figure 3. The predicted wavenumber of the amide I band is 1717 $cm^{-1}$ (Table 1),[32,33] and the band is narrow. This indicates that the large width of the observed amide I band in the actual spectra arises mostly from the wide distribution of intra- and interpolymer interactions, confirming our earlier conjecture. The predicted value differs by 4% or less from the experimental value of ca. 1790 $cm^{-1}$. The accuracy seems fair, if one considers that the calculation accounts only for one polymer side chain.

The amide II band is centered at 1540 $cm^{-1}$, which consists of 60% NH bending and 40% CN stretching.[32,43] The wavenumber of the amide II band is known to increase with increasing strength of the H-bond of the NH group. The observed CDMPC amide II band line shape has a shoulder, and hence it can also be separated into two bands (Figure 3), indicating two populations, with distributed wavenumbers of mainly N−H···O═C H-bonds, consistent with the amide I band. The wavenumber of the amide II band is lower in CDMPC than that in ADMPC by 2 $cm^{-1}$ (Table 1), indicating again slightly weaker H-bonds in CDMPC than in ADMPC. The NH stretch band is centered at 3300 $cm^{-1}$ and shows a significant shift from the "free" NH wavenumber of ca. 3600 $cm^{-1}$. This band shows consistent evidence of H-bonding of the NH groups. The amide III band, centered at 1213 $cm^{-1}$, for CDMPC is a combination of several vibrations[43] and is not examined in detail due to its complexity. Nonetheless, the slightly smaller wavenumber of the amide III band in CDMPC, compared to that in ADMPC, is consistent with the amide I and II results (Table 1). The predicted wavenumbers for amide bands II and III agree fairly well with the experimental values (Table 2). It is concluded that the nanostructures of the chiral cavities are different in CDMPC compared to those in ADMPC, with different strengths of H-bond distributions of the carbamate groups. This supports the hypothesis proposed by various researchers, based on chromatographic studies, that the molecular environments of these chiral cavities are different in the different polymers and one cause for the observed selectivity differences.

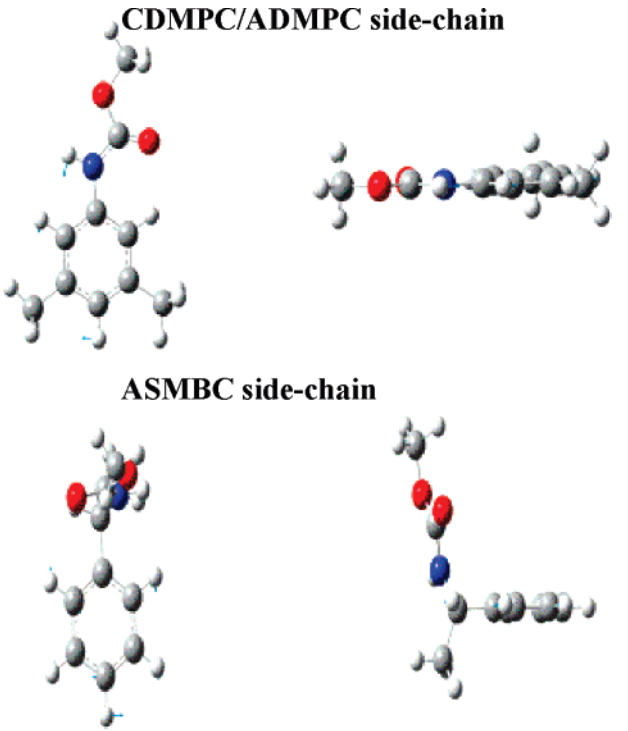


**Figure 4.** Optimized structures of CDMPC/ADMPC side chain and ASMBC side chain. The ASMBC side chain structure is predicted to have a nonplanar structure, or "kink", due to the tetrahedral carbon atom between the phenyl ring and NH group, resulting in the smaller end-to-end distance. Only one conformer is shown for ASMBC. The other conformer (see text) looks similar to the one shown.

For CDMPC, the band at 1614 $cm^{-1}$, with a shoulder at 1603 $cm^{-1}$, is due to the quadrant stretching of the phenyl ring carbon−carbon bonds.[44] These wavenumbers are the same as those in ADMPC (Table 1). These bands have significant intensities in both the CDMPC and ADMPC spectra, because of the $CH_3$ and NH groups attached to the phenyl rings. These substituents provide a substantial asymmetry to the phenyl vibrations, resulting in large changes in the transient dipole moments, and hence higher intensities of the phenyl bands.[44] The simulations confirm that the asymmetric and symmetric vibrations of the phenyl bands are coupled to the NH bending mode, resulting in enhancement of the phenyl intensities (Figure 4, see also Supporting Information). The detailed normal-mode analysis done with Gaussian software (also shown in the Supporting Information) shows that the phenyl bands have ca. 5% contribution from NH bending vibrations. The $CH_3$ substituents increase the $\pi$-basicity of the phenyl groups, resulting in $\pi-\pi$ interactions with the phenyl groups of the solutes.

*3.1.2. Effect of Side Chain: ASMBC versus ADMPC.* The IR spectrum of ASMBC is significantly different from that of CDMPC or ADMPC (Figure 3). For ASMBC, three overlapping peaks may be distinguished from the line shape of the amide I band. The wavenumbers of these bands are lower than those in ADMPC (Table 1). DFT simulations predict a nonplanar structure for the ASMBC side chain compared to a planar structure for the ADMPC/CDMPC side chain (Figure 4). Simulations predict a lower wavenumber for the non-H-bonded amide I in ASMBC than in ADMPC, consistent with the data (Table 1). Evidently, the small wavenumber shift in ASMBC is due mainly to the difference in side chain structure (Figures 1 and 4). The DFT optimized structure of the ASMBC side chain indicates that the C═O group interacts with the polar CH group of the same side chain, resulting in a lower amide I wavenumber. Moreover, the width of the amide I band in

ASMBC is slightly broader than that in the other two polymers, indicating that the H-bond distribution is broader in ASMBC. One of the reasons could be the presence of additional C═O···HC interactions in the side chains induced by the different packing of the polymer chains.

The amide II band in ASMBC has a broader distribution than those in ADMPC, consistent with the amide I results (Table 1). The amide II band in ASMBC has a lower wavenumber than that in ADMPC, possibly due to the lack of coupling at the phenyl groups. The predicted higher wavenumber of the amide III band for ASMBC compared to that of ADMPC is consistent with the data. DFT calculations predict two possible conformations for the ASMBC side chains, corresponding probably to two local energy minima (Table 1; see also Supporting Information), differing by only 0.06 kcal/mol and resulting in different wavenumbers for the amide bands I−III. The small differences in the wavenumbers of the amide bands of these two conformers can also cause them to overlap and cause the overall band to appear broader. The DFT-predicted intensities of the ASMBC phenyl groups are significantly smaller and agree well with the data. The lack of substituents on the ASMBC phenyl ring, compared to ADMPC, affects the basicity of the ring, resulting in different $\pi-\pi$ interactions with the solutes. The presence of the kink in the ASMBC side chain can also result in different packing arrangements (see section 3.2), resulting in different interactions with the solutes and solvents compared to ADMPC or CDMPC.

It is concluded that the strengths of the H-bonds of C═O and NH groups present in the chiral cavities of these polymers are significantly different. For CDMPC, the cavities are slightly bigger in size than for ADMPC, mainly due to the differences in the backbones, resulting in weaker intrapolymer H-bonds in the former. For ASMBC, the H-bond strengths of the C═O groups are stronger compared to ADMPC due to the interactions with the neighboring CH groups in the same side chains, even though ADMPC and ASMBC have the same backbone. The strengths of intrapolymer H-bonds of the C═O groups for these polymers are inferred to be in the following order: ASMBC > ADMPC > CDMPC. The strengths of the H-bonds of the NH groups for these polymers are inferred to be in the order ADMPC > CDMPC > ASMBC. The coupling of the NH and $CH_3$ groups with the phenyl ring results in much higher intensities of the phenyl peaks in ADMPC and CDMPC compared to ASMBC. This coupling results in different $\pi$-acidities and basicities of the phenyl rings, yielding different face-to-face and face-to-edge phenyl−phenyl interactions with the phenyl groups of the solutes. The presence of the kink in the ASMBC side chain can also result in a different local environment. These results confirm the hypothesis proposed by various researchers, based on chromatography results, that the C═O, NH, and phenyl groups have different molecular environments in the polymer chiral cavities.

**3.2. XRD Results.** It is found that the XRD spectra are independent of the coating solvent used (see section 2.3). Any small conformational change possibly due to the different coating solvent does not result in any significant difference in the XRD spectra. The XRD spectra of all three polymers show evidence of crystallinity (Figure 5). Since the polymer films showed birefringence in polarized optical microscopy, it is inferred that they are partially ordered. The ADMPC spectrum, shown here for reference,[32] has a broad peak with a *d*-spacing centered at 15.5 Å and a 3.5 Å width (Table 2), indicating that the polymer film is partially crystalline but substantially amorphous. Our hypothesis is that the observed spacing corresponds to the repeat distance between the helical polymer chains, which interpenetrate slightly, generating some of the weak interpolymer interactions inferred from the IR results.[32]

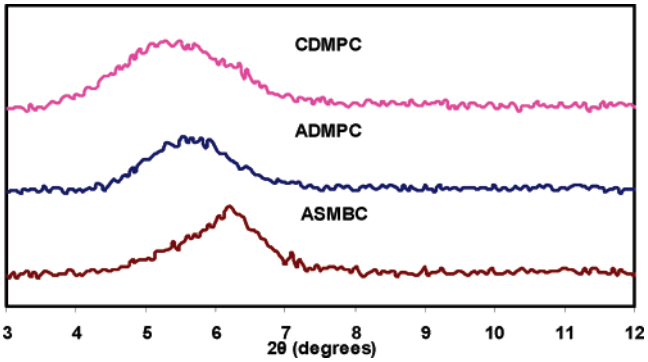


**Figure 5.** XRD patterns of CDMPC, ADMPC, and ASMBC polymers. The *d*-spacings and peak widths are shown in Table 2.

**Table 2.** XRD *d*-Spacings for Polymers in the Dry State (see Figure 5)

| polymer | *d*-spacing, Å | fwhm,[a] Å |
|---|---|---|
| ADMPC | 15.5 | 3.5 ± 0.5 |
| CDMPC | 16.3 | 4.5 ± 0.5 |
| ASMBC | 14.1 | 2.5 ± 0.5 |

[a] Full width at half-maximum.

The XRD pattern for the CDMPC polymer has a broad peak at 16.3 ± 4.5 Å. The slightly higher *d*-spacing suggests a larger distance between the polymer chains and can be attributed to the differences in their polymer backbones. The XRD pattern for ASMBC has a narrower peak at 14.1 ± 2.5 Å, indicating that the ASMBC may be slightly more ordered or may have larger crystallites than ADMPC or CDMPC. The lower *d*-spacing indicates a smaller distance between the polymer chains. This can be attributed to the clearly predicted slight kink in the ASMBC side chain structure (Figure 4) if one assumes that ADMPC and ASMBC have almost the same backbone helicities (see CP/MAS NMR results in section 3.3).

The XRD results show that the packing arrangements are different in the three polymers, resulting in different interpenetrations of the adjacent polymer chains. The larger distance between two adjacent chains for CDMPC compared to ADMPC can result in weaker H-bonds. The differences in the packing arrangements of the polymer chains result in different nanostructures of the chiral cavities.

**3.3. CP/MAS Solid-State NMR Results.** *3.3.1. Effect of Backbone: CDMPC versus ADMPC.* The $^{13}C$ CP/MAS NMR spectra of the CDMPC and ADMPC thin films on porous silica beads are shown in Figure 6. The polymer spectra with no silica beads were also obtained and show no differences. The ADMPC spectrum is shown here for comparison[27,32] and is also analyzed in detail. For the ADMPC side chains, the following peaks are seen (Figures 1 and 6, Table 3): one $CH_3$ peak; three phenyl peaks, Ph II, III, and IV (peak Ph I is observed only in MAS but not in CP/MAS; see Figure 7 and section 3.4); and one C═O peak.[27,32] The observed $^{13}C$ resonances are broad, mainly due to the partially ordered polymer structure inferred from the XRD results. This structure apparently results in a wide distribution of local molecular environments and chemical shifts for each carbon.[32,45]

The side chain peaks for CDMPC, $CH_3$ and Ph II−IV, are quite similar to those of ADMPC. The phenyl Ph II peak is slightly broader in CDMPC than in ADMPC, possibly due to the differences in the packing arrangements of the two polymers,

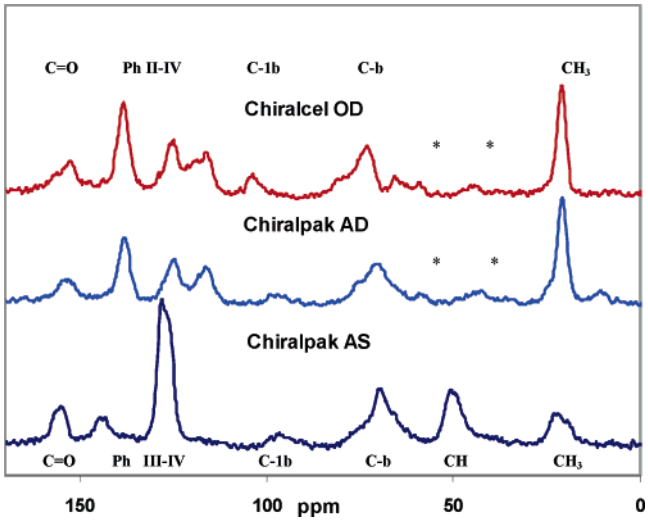


**Figure 6.** $^{13}C$ CP/MAS solid-state NMR spectra of Chiralcel OD (CDMPC-coated silica beads), Chiralpak AD (ADMPC-coated silica beads), and Chiralpak AS (ASMBC-coated silica beads). Assignments and chemical shifts are shown in Table 3. Spinning side bands are indicated by asterisks.

resulting in different environments for the phenyl groups. For the C═O peak, a slightly lower chemical shift is observed for CDMPC than for ADMPC, indicating that the H-bonds are slightly weaker in the former, consistently with the IR results.[32,46] The C═O peak is slightly sharper in CDMPC, probably because the H-bond distribution is narrower.

The DFT-predicted chemical shifts, for one side chain of either CDMPC or ADMPC, agree fairly well with the data (Table 3). These simulations, which correspond to completely free C═O and NH groups with no intra- or interpolymer H-bonds, show narrow peaks. Therefore, the large width of the observed C═O peak arises mostly from the wide distribution of intra- and interpolymer interactions, which affect the electronic environment of C═O, supporting our previous conclusion. The H-bonding of C═O (see IR data) can affect the resonance frequency of the carbon atom, resulting in ca. 4% discrepancy between the observed and simulated chemical shifts.

The chemical shifts of the backbone carbons are analyzed in detail, because they provide information on the glycosidic bonds and the polymer helicity. The chemical shifts of the C-1 to C-6 backbone peaks (Figures 1 and 6) show some significant differences between CDMPC and ADMPC. CDMPC has three peaks at 66, 73, and 80 ppm. The peak at 66 ppm is due to the C-6 resonance; the broad peak at 73 ppm in CDMPC includes the C-2, C-3, and C-5 resonances; and the peak at 80 ppm is due to the C-4 resonance. These peaks are assigned on the basis of the literature spectra of cellulose and cellulose triacetate as follows. Cellulose, which forms a single 2-fold helix, also shows three peaks in the 60−95 ppm region.[47] The C-6 resonance appears at 67 ppm; the C-2, C-3, and C-5 resonances are in the 70−80 ppm range; and the C-4 resonance appears at 91 ppm.[47] For derivatized cellulose triacetate, the C-6 resonance appears at 62 ppm (slightly upfield compared to cellulose); the C-2, C-3, and C-5 resonances remain in the 70−80 ppm range; and the C-4 resonance appears at 80 ppm (significantly upfield).[48] The shifts in the C-4 and C-6 resonances are due mainly to the cellulose derivatization, if one presumes that the helicity of the cellulose triacetate is the same as that of cellulose.[49] Since the type of the derivatized group (carbamate rather than acetate) is expected to affect only slightly these chemical shifts, similar trends are expected in the CDMPC shifts for the backbone carbon resonances.

The C-1 peak of CDMPC is broad and is centered at 104 ppm (Figure 6). The C-1 resonance appears at 106−108 ppm for cellulose and shifts to 100−103 ppm for cellulose triacetate. The cellulose carbamate forms a 3-fold single helix,[24] and the cellulose triacetate forms a 2-fold helix.[49] In order to understand further the observed chemical shifts for the C-1 resonance, DFT simulations were performed for cellulose monomer (with no glycosidic bonds) and cellulose dimer (with one glycosidic bond per dimer). The predicted chemical shift for the $\beta$-anomeric C-1 carbon in cellulose was 107 ppm. The predicted C-1 shift for the cellulose acetate monomer was 106 ppm. The C-1 chemical shift of the cellulose dimer with 3-fold helicity is 103−106 ppm, which agrees with the data. Hence, the simulations and data support the hypothesis of a 3-fold helical conformation for CDMPC.

ADMPC has two peaks (at 71 and 76 ppm) in the 60−95 ppm region, compared to three for CDMPC. This is attributed to the differences in their backbones, with boat or chair conformations, which affect their glycosidic linkages. V-amylose, which forms a single 6-fold helix, has three peaks in the 60−90 ppm region.[50] The C-6 resonance appears at ca. 61 ppm; the C-2, C-3, and C-5 resonances appear in the 70−80 ppm range; and the C-4 resonance appears at ca. 82 ppm.[50] Upon derivatization to amylose acetate or amylose sulfate, which are single helices with less than 6-fold helix,[51] the C-2, C-3, C-5, and C-6 peaks remain in the same range, with small shifts compared to the corresponding peaks in V-amylose.[52] For ADMPC, these resonances appear to overlap with one broad peak of 71 ppm. The shoulder at 76 ppm corresponds to the C-4 resonance. It is concluded that the C-4 peak moves upfield for CDMPC and ADMPC, compared to cellulose and amylose, respectively, mainly due to changes in the glycosidic conformation. The peak broadening is due to the partial crystallinity of ADMPC.[32] It has been shown that, upon absorption of a polar solvent, the backbone peaks become better resolved due to the increase in polymer crystallinity.[27,32]

The C-1 peak of ADMPC is also broad and is centered at 97 ppm (Figure 6), whereas the C-1 peak in V-amylose appears at 103 ppm.[50] The peak is known to move upfield in derivatized amylose polymer.[52] The shift can be due to one of two possible effects. The first is that the derivatization at the C-2 site affects the C-1 chemical shift.[52] The second is that the glycosidic linkage changes from 6-fold to lower-fold. A- and B-amylose have C-1 peaks at 99−101 ppm, because they form double helices.[50] It is assumed that ADMPC forms a single helix, because of its bulky side chains (Figure 2), which may hinder it from forming a double helix, and since most of the derivatized amylose polymers (e.g., esters) seem to form single helices upon derivatization. In CDMPC or ADMPC, the observed broad C-1 peak corresponds to wide distributions of local molecular environments, since the polymer is partially ordered.[32,50]

The DFT-predicted chemical shift for the α-anomeric C-1 resonance in amylose monomer was 105 ppm. For $\beta$-anomeric C-1 carbon in cellulose, the effect of the substituent is less significant compared to the α-anomeric C-1 in amylose, with the resonance of the $\beta$-anomeric C-1 atom being observed downfield from the resonance of the α-anomeric C-1 atom (105 vs 107 ppm).[53] A value of 102 ppm is predicted for the amylose acetate monomer C-1 resonance. The shift from 105 to 102 ppm is due to the acetate group substituent. DFT simulations for the amylose dimer, by use of conformation angles of 4-fold helicity, and results in predicted values for the C-1 resonance of 96−99 ppm, which are in agreement with the ADMPC data. The simulations show that changes in the glycosidic linkage

**Table 3.** Measured and Predicted Chemical Shifts of $^{13}C$ Peaks for the Polymers[a]

| | | | | | phenyl peaks | | | | |
|---|---|---|---|---|---|---|---|---|---|
| | $CH_3$ | CH-s[b] | CH-b[b] | C1-b[b] | I | II | III | IV | C=O |
| Chiralpak OD or CDMPC-coated silica beads | 21 (21) | N/A | 68, 73, 80[c] | 104[c] | N/O (112) | 117[c] | 125 | 138 (138) | 152[c] |
| Chiralpak AD or ADMPC-coated silica beads | 21 (21) | N/A | 71, 76[c] | 97[c] | N/O (111) | 116 | 125 | 138 (139) | 154[c] |
| *predicted for ADMPC/CDMPC side chain*[d] | *23, 24* | *N/A* | *N/A* | *N/A* | *N/O* | *116, 117* | *127* | *144, 147* | *157* |
| Chiralpak AS or ASMBC-coated silica beads | 23[c] (23) | 51[c] (50) | 70[c] | 97[c] | N/O (112) | N/A | 127, 129 (127, 129) | 144[c] | 156[c] |
| *predicted for ASMBC side chain*[d] | *19, 26* | *54, 57* | *N/A* | *N/A* | *N/O* | *N/A* | *128−135, 128−132* | *148, 152* | *159, 159* |

[a] Peaks are from CP/MAS and MAS solid-state NMR. Chemical shifts in parts per million, ±1 ppm, with glycine as a reference are listed; see Figures 6 and 7. Only the peaks observed in MAS $^{13}C$ spectra in Figure 7 are shown in parentheses. N/O, not observed; N/A, not available [b] b = backbone of the polymer; s = side chain of the polymer. [c] Peaks too broad to establish chemical shift accurately; see text. [d] Chemical shifts for polymer side chains are predicted at the DFT/B3LYP/6-311+g(d,p) level of theory (shown in italic type).

conformation affect the C-1 chemical shift more than the substituent (102 vs 96−99 ppm). This is in agreement with the suggestion by Gidley and Bociek[50] that the C-1 chemical shift is primarily determined by the glycosidic linkage conformation.[54] Hence, our simulations support the hypothesis of a 4-fold helical conformation for ADMPC.

*3.3.2. Effect of Side Chain: ASMBC versus ADMPC.* For ASMBC, one broad peak is observed for the backbone C-2 to C-6 resonances (Figure 6). The C-1 resonance is centered at 97 ppm, similar to that of ADMPC, indicating that these polymers have similar glycosidic linkage conformations and possibly similar helicities. This also supports our hypothesis that the *d*-spacing observed in XRD results mainly corresponds to the distance between the polymer chains and not to the pitch of the helix.

The peaks due to side chains differ significantly, however. The $CH_3$ peak in ASMBC has a smaller intensity and is shifted slightly upfield compared to the $CH_3$ peak in ADMPC. ASMBC also has a peak at 50 ppm corresponding to the CH groups in its side chain. Only two phenyl peaks are observed in ASMBC, but there are three in ADMPC. The Ph III peak is assigned to the five phenyl carbons that are not connected to the CH group (Figure 1). The Ph IV peak is assigned to the carbon connected to CH. The C=O peak is shifted downfield in ASMBC, compared to that in ADMPC, indicating that the strength of the H-bond is higher in ASMBC, consistent with the IR results.

DFT simulations show that the chemical shifts of the CH and the phenyl C-a carbon (see Figure 1) depend on the side chain conformation. These conformations result in significantly different chemical shifts for the CH and Ph C-a carbons but not for the other peaks. In one possible conformer, the chemical shifts of the $CH_3$ peak differ from the data by +4 ppm, and in the second conformer, by −3 ppm. Possibly there are several conformers, causing the observed NMR peak broadenings, consistent with the IR results.

The differences in the chemical shifts (~7 ppm) of the C-1 resonances of CDMPC and ADMPC indicate that the backbones of these polymers have significantly different helicities. By contrast, the C-1 resonances of ADMPC and ASMBC differ by less than 1 ppm, indicating similar helicities. This may be a major factor underlying the differences in the chiral discrimination behavior for various chiral solutes, as suggested previously by various researchers mostly on the basis of chromatography results. Helicity differences can also affect the inter- and intra-polymer H-bonds strengths, which in turn affect the chemical shifts and the widths of the C=O resonances, and the IR wavenumbers (see section 3.1).

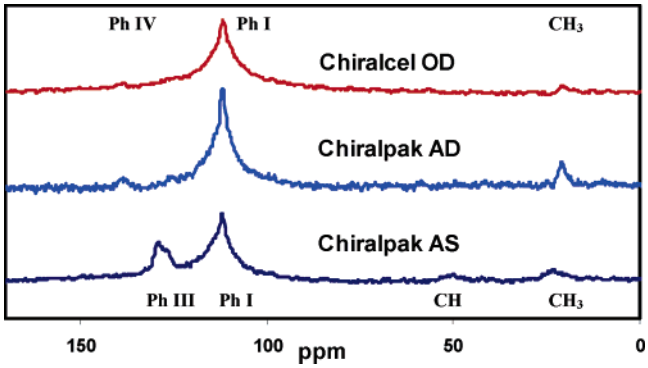


**Figure 7.** $^{13}C$ MAS solid-state NMR spectra of Chiralcel OD (CDMPC-coated silica beads), Chiralpak AD (ADMPC-coated silica beads), and Chiralpak AS (ASMBC-coated silica beads).

**3.4. MAS Solid-State NMR Results.** MAS and CP/MAS $^{13}C$ spectra generally show quite different intensities for the same carbons, because each technique reflects one extreme of molecular motion, fast or slow.[32,55] The backbone peaks are not observed in these MAS spectra (Figure 7), indicating that the backbones of all three polymers have no substantial molecular mobilities.

Only the phenyl and $CH/CH_3$ peaks of the side chains are resolved and observed, indicating, as expected, that the side chains are more mobile than the backbone. The phenyl peak Ph I is observed, in contrast to the CP/MAS spectra, probably because the contact time (0.8 ms) may be adequate for observing this fast-tumbling group. For CDMPC and ADMPC, the three phenyl peaks (II−IV) observed in the MAS spectra are broader than in their respective CP/MAS spectra. DFT simulations of monomers or dimers show no Ph I peak. The observed peak in the actual spectrum may, therefore, arise from the complex packing arrangements of the polymer chains not accounted for in the simulations. Overall, the combined MAS and CP/MAS results provide information about the state of molecular motion and the crystallinity in these polymers. From this information as a baseline, one may start elucidating the effects of solvents and chiral solutes on the polymeric structures and link such effects to the molecular geometries and physics of molecular recognition processes.

## 4. Conclusions

The effects of the backbone and side chain on the molecular environments of the chiral cavities in three commercially important polysaccharide based chiral sorbents are studied by

ATR-IR, XRD, $^{13}C$ CP/MAS and MAS solid-state NMR, and DFT modeling. It is concluded that the strengths of H-bonds of the C═O and NH groups in the chiral cavities of these polymers are significantly different. For CDMPC, the cavities are slightly bigger than for ADMPC, mainly due to the differences in the polymer backbones, resulting in weaker intrapolymer H-bonds in the former. For ASMBC, the H-bond strengths of the C═O groups are stronger than for ADMPC, even though they have the same backbones, because of the interactions with the neighboring CH groups in the same side chains. The strengths of the H-bonds of C═O groups for these polymers are inferred to be in the following order: ASMBC > ADMPC > CDMPC. The strengths of the H-bonds of the NH groups are inferred to be in the order ADMPC > CDMPC > ASMBC. The coupling of the NH and $CH_3$ groups with the phenyl ring results in much higher IR intensities in ADMPC and CDMPC than in ASMBC. XRD results show different *d*-spacings between the polymer chains in the three polymers, resulting in variations in the packing arrangements, and different intra- and interpolymer interactions between the C═O and NH groups. From the NMR chemical shifts of the C-1 carbon, it is inferred that the backbone glycosidic bond conformations and helicities are similar for ADMPC and ASMBC but different for ADMPC and CDMPC. DFT simulations predict that the ADMPC and CDMPC side chains have a planar conformation, while the ASMBC side chain has nonplanar, and possibly multiple, conformations. Hence, the C═O, NH, and phenyl groups in the chiral cavities of these polymers have different molecular environments, which may be a major factor affecting the selectivities of chiral solutes.

**Acknowledgment.** We thank Dr. Geoffery Cox from Chiral Technologies (West Chester, PA) for supplying the Chiralpak AD, Chiralpak AS, and Chiralcel OD silica beads. Computational resources were obtained through the supercomputing facility at Purdue University. We thank Dr. Yury Zvinevich (School of Chemical Engineering, Purdue University) for help in the solid-state NMR experiments. We thank Ms. Siao Yee Wee and Mr. Ji Xian Loh for help in the IR experiments and Dr. Srinivas Janaswamy (Department of Food Sciences, Purdue University) for help in generating the polymer helical structures. This research was supported in part by an NSF grant, CTS-0625189.

**Supporting Information Available.** Three Gaussian 03 output files showing the optimized structures, and the IR vibrations for (i) one CDMPC/ADMPC and (ii, iii) two ASMBC side chain conformations. This material is available free of charge via the Internet at http://pubs.acs.org.

## References and Notes

(1) Delaage, M. *Molecular Recognition Mechanisms*; VCH Publishers, Inc.: New York, 1991.
(2) Jinno, K. *Chromatographic Separations Based on Molecular Recognition*; John Wiley & Sons: New York, 1997.
(3) Francotte, E. R. *J. Chromatogr. A* **2001**, *906*, 379.
(4) Pirkle, W. H.; House, D. W.; Finn, J. M. *J. Chromatogr.* **1980**, *192*, 143.
(5) Okamoto, Y.; Aburatani, R.; Fukumoto, T.; Hatada, K. *Chem. Lett.* **1987**, *9*, 1857.
(6) Thelohan, S.; Jadaud, P.; Wainer, I. W. *Chromatographia* **1989**, *28*, 551.
(7) Armstrong, D. W.; Tang, Y. B.; Chen, S. S.; Zhou, Y. W.; Bagwill, C.; Chen, J. R. *Anal. Chem.* **1994**, *66*, 1473.
(8) Lammerhofer, M.; Lindner, W. *J. Chromatogr. A* **1996**, *741*, 33.
(9) Yamamoto, C.; Okamoto, Y. *Bull. Chem. Soc. Jpn.* **2004**, *77*, 227.
(10) Okamoto, Y.; Yashima, E. *Angew. Chem., Int. Ed.* **1998**, *37*, 1021.
(11) Ye, Y. K.; Stringham, R. W. *Chirality* **2006**, *18*, 519.
(12) Ali, I.; Aboul-Enein, H. Y. *J. Sep. Sci.* **2006**, *29*, 762.
(13) Ellington, J. J.; Evans, J. J.; Prickett, K. B.; Champion, W. L. *J. Chromatogr. A* **2001**, *928*, 145.
(14) Goossens, J. F.; Foulon, C.; Villard, A. L.; Puy, J. Y.; Lefebvre, I.; Perigaud, C.; Vaccher, C.; Bonte, J. P. *Biomed. Chromatogr.* **2005**, *19*, 415.
(15) Cass, Q. B.; Batigalhia, F. *J. Chromatogr. A* **2003**, *987*, 445.
(16) Collina, S.; Loddo, G.; Urbano, M.; Rossi, D.; Mamolo, M. G.; Zampieri, D.; Alcaro, S.; Gallelli, A. A.; Azzolina, O. *Chirality* **2006**, *18*, 245.
(17) Lipka-Belloli, E.; Len, C.; Mackenzie, G.; Ronco, G.; Bonte, J. P.; Vaccher, C. *J. Chromatogr. A* **2002**, *943*, 91.
(18) Visentin, S.; Amiel, P.; Gasco, A.; Bonnet, B.; Suteu, C.; Roussel, C. *Chirality* **1999**, *11*, 602.
(19) Kennedy, J. H. *J. Chromatogr. A* **1996**, *725*, 219.
(20) Ye, Y. K.; Stringham, R. W.; Wirth, M. J. *J. Chromatogr. A* **2004**, *1057*, 75.
(21) Wang, T.; Chen, Y. D. W.; Vailaya, A. *J. Chromatogr. A* **2000**, *902*, 345.
(22) Chen, T. K.; Mills, R. J. *J. Chromatogr. A* **1994**, *659*, 321.
(23) Booth, T. D.; Lough, W. J.; Saeed, M.; Noctor, T. A. G.; Wainer, I. W. *Chirality* **1997**, *9*, 173.
(24) Vogt, U.; Zugenmaier, P. *Ber. Bunsen-Ges.-Phys. Chem. Chem. Phys.* **1985**, *89*, 1217.
(25) Yamamoto, C.; Yashima, E.; Okamoto, Y. *Bull. Chem. Soc. Jpn.* **1999**, *72*, 1815.
(26) Vogt, U.; Zugenmaier, P. Communication at the European Science Foundation Workshop on Specific Interaction in Polysaccharide Systems, 1983, Uppsala, Sweden.
(27) Wenslow, R.; Wang, T. *Anal. Chem.* **2001**, *73*, 4190.
(28) Yamamoto, C.; Yashima, E.; Okamoto, Y. *J. Am. Chem. Soc.* **2002**, *124*, 12583.
(29) Chankvetadze, B.; Yashima, E.; Okamoto, Y. *J. Chromatogr. A* **1994**, *670*, 39.
(30) Chankvetadze, B.; Yashima, E.; Okamoto, Y. *J. Chromatogr. A* **1995**, *694*, 101.
(31) Wang, T.; Wenslow, R. *J. Chromatogr. A* **2003**, *1015*, 99.
(32) Kasat, R. B.; Zvinevich, Y.; Hillhouse, H. W.; Thomson, K. T.; Wang, N. H. L.; Franses, E. I. *J. Phys. Chem. B* **2006**, *110*, 14114.
(33) Kasat, R. B.; Chin, C. Y.; Thomson, K. T.; Franses, E. I.; Wang, N. H. L. *Adsorption* **2006**, *12*, 405.
(34) Campbellsmith, P. J.; Arnott, S. *Acta Crystallogr. A* **1978**, *34*, 3.
(35) *Discover*, 3.0 ed.; Accelrys, Inc.: San Diego, CA.
(36) Sun, H.; Mumby, S. J.; Maple, J. R.; Hagler, A. T. *J. Phys. Chem.* **1995**, *99*, 5873.
(37) Frisch, M. J.; Trucks, G. W.; Schlegel, H. B.; Scuseria, G. E.; Robb, M. A.; Cheeseman, J. R.; Montgomery, J. A., Jr.; Vreven, T.; Kudin, K. N.; Burant, J. C.; Millam, J. M.; Iyengar, S. S.; Tomasi, J.; Barone, V.; Mennucci, B.; Cossi, M.; Scalmani, G.; Rega, N.; Petersson, G. A.; Nakatsuji, H.; Hada, M.; Ehara, M.; Toyota, K.; Fukuda, R.; Hasegawa, J.; Ishida, M.; Nakajima, T.; Honda, Y.; Kitao, O.; Nakai, H.; Klene, M.; Li, X.; Knox, J. E.; Hratchian, H. P.; Cross, J. B.; Bakken, V.; Adamo, C.; Jaramillo, J.; Gomperts, R.; Stratmann, R. E.; Yazyev, O.; Austin, A. J.; Cammi, R.; Pomelli, C.; Ochterski, J. W.; Ayala, P. Y.; Morokuma, K.; Voth, G. A.; Salvador, P.; Dannenberg, J. J.; Zakrzewski, V. G.; Dapprich, S.; Daniels, A. D.; Strain, M. C.; Farkas, O.; Malick, D. K.; Rabuck, A. D.; Raghavachari, K.; Foresman, J. B.; Ortiz, J. V.; Cui, Q.; Baboul, A. G.; Clifford, S.; Cioslowski, J.; Stefanov, B. B.; Liu, G.; Liashenko, A.; Piskorz, P.; Komaromi, I.; Martin, R. L.; Fox, D. J.; Keith, T.; Al-Laham, M. A.; Peng, C. Y.; Nanayakkara, A.; Challacombe, M.; Gill, P. M. W.; Johnson, B.; Chen, W.; Wong, M. W.; Gonzalez, C.; Pople, J. A. *Gaussian 03*, Revision C.02; Gaussian, Inc.: Wallingford, CT, 2004.
(38) Becke, A. D. *J. Chem. Phys.* **1993**, *98*, 5648.
(39) Meyer, M.; Steinke, T.; Brandl, M.; Suhnel, J. *J. Comput. Chem.* **2001**, *22*, 109.
(40) Scheiner, S. *Hydrogen Bonding: a Theoretical Perspective*; Oxford University Press: New York, 1997.
(41) Andersson, M. P.; Uvdal, P. *J. Phys. Chem. A* **2005**, *109*, 2937.
(42) Yashima, E.; Sahavattanapong, P.; Okamoto, Y. *Chirality* **1996**, *8*, 446.
(43) Bellamy, L. J. *The Infra-red Spectra of Complex Molecules*, 3rd ed.; Wiley: New York, 1975.
(44) Colthup, N. B.; Daly, L. H.; Wiberley, S. E. *Introduction to Infrared and Raman Spectroscopy*, 3rd ed.; Academic Press: Boston, MA, 1990.
(45) Atalla, R. H.; Vanderhart, D. L. *Science* **1984**, *223*, 283.
(46) Ando, S.; Ando, I.; Shoji, A.; Ozaki, T. *J. Am. Chem. Soc.* **1988**, *110*, 3380.

(47) Kono, H.; Erata, T.; Takai, M. *J. Am. Chem. Soc.* **2002**, *124*, 7512.
(48) Kono, H.; Yunoki, S.; Shikano, T.; Fujiwara, M.; Erata, T.; Takai, M. *J. Am. Chem. Soc.* **2002**, *124*, 7506.
(49) Sikorski, P.; Wada, M.; Heux, L.; Shintani, H.; Stokke, B. T. *Macromolecules* **2004**, *37*, 4547.
(50) Gidley, M. J.; Bociek, S. M. *J. Am. Chem. Soc.* **1988**, *110*, 3820.
(51) Zugenmaier, P.; Steinmeier, H. *Polymer* **1986**, *27*, 1601.
(52) Richter, A.; Wagenknecht, W. *Carbohydr. Res.* **2003**, *338*, 1397.
(53) Hewitt, J. M.; Linder, M.; Perez, S.; Buleon, A. *Carbohydr. Res.* **1986**, *154*, 1.
(54) Horii, F.; Yamamoto, H.; Hirai, A.; Kitamaru, R. *Carbohydr. Res.* **1987**, *160*, 29.
(55) Zeigler, R. C.; Maciel, G. E. *J. Phys. Chem.* **1991**, *95*, 7345.

BM070006H